Results from the NASA GSFC and LaRC Ozone Lidar Intercomparison: New Mobile Tools for Atmospheric Research

JOHN T. SULLIVAN*

Department of Atmospheric Physics, University of Maryland, Baltimore County, and Joint Center for Earth Systems Technology, Baltimore, Maryland

THOMAS J. MCGEE

Atmospheric Chemistry and Dynamics Laboratory, NASA Goddard Space Flight Center, Greenbelt, Maryland

RUSSELL DEYOUNG

Science Directorate, NASA Langley Research Center, Hampton, Virginia

LAURENCE W. TWIGG, GRANT K. SUMNICHT, DENIS PLIUTAU, AND TRAVIS KNEPP

Science Systems and Applications, Inc., Lanham, Maryland

WILLIAM CARRION

Coherent Applications Inc., Hampton, Virginia

(Manuscript received 1 October 2014, in final form 14 July 2015)

ABSTRACT

During a 2-week period in May 2014, the National Aeronautics and Space Administration (NASA) Goddard Space Flight Center Tropospheric Ozone Differential Absorption Lidar (GSFC TROPOZ DIAL) was situated near the NASA Langley Research Center (LaRC) Mobile Ozone Lidar (LMOL) and made simultaneous measurements for a continuous 15-h observation period in which six separate ozonesondes were launched to provide reference ozone profiles. Although each of these campaign-ready lidars has very different transmitter and receiver components, they produced very similar ozone profiles, which were mostly within 10% of each other and the ozonesondes. The observed column averages as compared to the ozonesondes also agree well and are within 8% of each other. A robust uncertainty analysis was performed, and the results indicate that there is no statistically significant systematic bias between the TROPOZ and LMOL instruments. With the extended measurements and ozonesonde launches, this intercomparison has yielded an in-depth evaluation of the precision and accuracy of the two new lidars. This intercomparison is also the first (to the best of the authors' knowledge) reported measurement intercomparison of two ground-based tropospheric ozone lidar systems within the United States.

1. Introduction

The Goddard Space Flight Center Tropospheric Ozone Differential Absorption Lidar (GSFC TROPOZ DIAL) and the Langley Research Center (LaRC) Mobile Ozone Lidar (LMOL) instruments have been developed through the National Aeronautics and Space Administration (NASA) in order to measure the vertical distribution of tropospheric ozone within their respective urban regions. Specifically, these lidars have been developed as part of the ground-based Tropospheric Ozone Lidar Network (TOLNet), which currently consists of five stations across the United States (http://www-air.larc.nasa.gov/missions/TOLNet/).

Most ground-based ozone lidar systems have validated their ozone retrievals by comparisons with observations

* Current affiliation: Atmospheric Chemistry and Dynamics Branch, NASA Goddard Space Flight Center, Greenbelt, Maryland, and Oak Ridge Associated Universities, Oak Ridge, Tennessee.

Corresponding author address: John T. Sullivan, Atmospheric Chemistry and Dynamics Branch, NASA Goddard Space Flight Center, Mail Code 614, Greenbelt, MD 20771.
E-mail: john.t.sullivan@nasa.gov

DOI: 10.1175/JTECH-D-14-00193.1

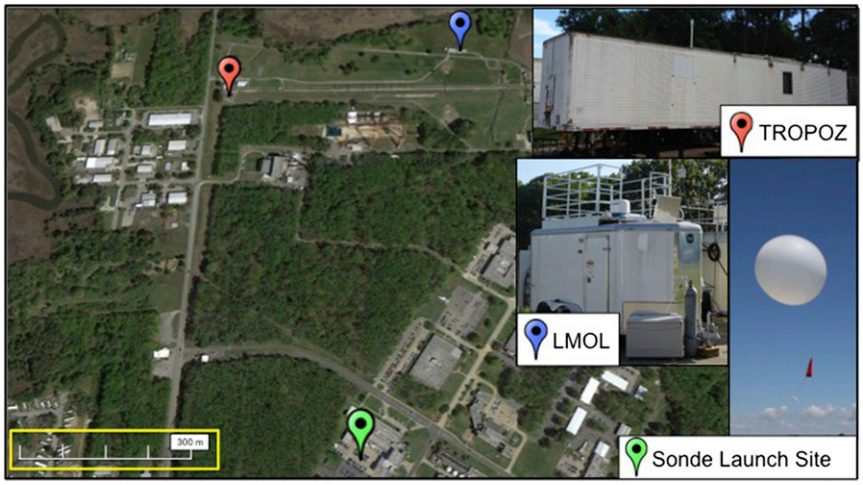

FIG. 1. System locations at LaRC for the GSFC TROPOZ DIAL (TROPOZ, red marker), LMOL (blue marker), and the ozonesonde launch site (sonde launch site, green marker). The scale of the map in the bottom-left corner denotes 300 m. An image of each of the transportable trailers is shown in the inset figure.

from balloonborne electrochemical concentration cell (ECC) ozonesondes launched from collocated sites. However, the sondes can be carried great distances away from the lidar site by the prevailing winds, which can complicate the comparison, because the lidar and sonde observations are made at different locations. A side-by-side comparison between two ozone lidars ensures that both instruments sample nearly the same atmospheric volume and provides the opportunity for a continuous, longer-term ozone profile comparison. Because each of these mobile systems have been operational for less than a year, a joint NASA GSFC–LaRC lidar campaign was performed to ensure a quantitative assessment of the retrieval accuracy and precision, as well as an assurance of the campaign readiness of each system. For these reasons, the TROPOZ and the LMOL made simultaneous and collocated measurements of essentially the same atmospheric volume for a continuous 15-h observation period (0400–1918 UTC 4 May 2014) in which six separate ECC sondes served as reference ozone profiles.

Figure 1 shows an overview of the deployment locations at the NASA LaRC in Hampton, Virginia. The TROPOZ was located at 37.102°N, 76.392°W, 4 m MSL (red marker), and the LMOL (blue marker) was located 540 m to the east. The ECC sonde launch site (green marker) was located 840 m southeast of TROPOZ.

Although each of these transportable instruments has unique transmitter and receiver configurations, a similar ozone concentration profile may be obtained with a proper retrieval. The TROPOZ transmitter produces a much more energetic pulse (nearly 300 times more) at a lower repetition rate than the LMOL transmitter, which enables the TROPOZ to routinely resolve ozone in the upper free troposphere and beyond the tropopause. Conversely, the LMOL transmitter has a much higher repetition rate (20 times as fast) and a higher range resolution, which may be used in the future to characterize finescale temporal features of tropospheric ozone. Because of these differences, this intercomparison has served as an assurance of the quality and robustness of the individual hardware components and their ability to transmit and detect the necessary amount of signal to produce accurate ozone profiles. Important issues regarding both hardware and software have been identified, some of which may not have been discovered without this intercomparison.

The intercomparison began with each research group performing a nearly identical retrieval on the same set of raw signals to test whether the two retrievals would yield the same answers within acceptable limits. Following that, each group carefully examined their individual retrieval on their own set of data during specific time intervals. These retrievals were then quantitatively compared to each ECC sonde. A comparison of the time series data was performed that emphasizes each instrument's ability to characterize the evolution and dynamics of ozone during the observation period. The analysis continued with a relative difference plot of the time series data and a comparison of the average column ozone within the observation range. A statistical analysis was also performed to help quantify the agreement between retrievals.

There have been numerous successful stratospheric ozone lidar intercomparisons (McDermid et al. 1990; Steinbrecht et al. 2009) that focus on longer-duration (120-min average) comparisons, but because of ozone's

TABLE 1. Hardware and channel characteristics of the TROPOZ and LMOL. The retrieval vertical resolution for the range resolution is found in Fig. 4.

	TROPOZ	LMOL
Trailer dimensions (L × W × H; m)	13 × 3 × 4.5	5 × 2.5 × 3.5
Online wavelength (nm)	288.9	287.09
Offline wavelength (nm)	299.1	292.70
Transmitter	Nd:YAG	Nd:YLF pumped
	Raman-pumped H_2 and D_2 cell	Tunable Ce:LiCAF
Laser repetition rate (Hz)	50	1000
Transmit energy	12 mJ (299)/16 mJ (289)	50 μJ (287.09)/50 μJ (292.70)
Far-field receiver	Newtonian reflector	Newtonian reflector
	45-cm primary parabolic	40-cm primary parabolic
Retrieval height (km)	2.75–12	1.5–7
FOV (mrad)	1.0	1.4
Detection method	PC	PC
Photomultiplier type	Hamamatsu 7400P-03	Hamamatsu 7400U-03
Near-field receiver	Refractor	Newtonian reflector
	2.5-cm lens	40-cm primary parabolic
Retrieval height	350 m–3.25 km	500 m–2.5 km
FOV (mrad)	10.0	1.4
Detection method	PC	AN
Photomultiplier type	Hamamatsu 7400P-03	Hamamatsu 7400U-03
Interference filters	Materion	Barr
Center wavelengths (nm)	299.1 ± 0.25, 288.9 ± 0.25	285.0–302.5
FWHM (nm)	≤1.2	≤17.5
Data acquisition		
Licel transient recorder	Model PR 20	Model TR 20–80 (12-bit)
Max PC rate	250-MHz maximum	250-MHz maximum
AN detection rate	—	20-MHz maximum
Range resolution	100 ns–15 m	50 ns–7.5 m

shorter lifetime, smaller-scale transport, and mixing processes within the PBL and free troposphere, it is necessary to analyze tropospheric ozone at time scales on the order of several minutes. For measurements within TOLNet to be successful, especially with different instrument parameters and geographical locations, it will be necessary to ensure the quality of the results by intercomparisons.

The intercomparison results presented here show that although the TROPOZ and the LMOL have very different transmitter and receiver characteristics, they were able to produce very similar ozone profiles, demonstrating that each of these new instruments is campaign ready and suitable for measuring ozone throughout the PBL and free troposphere. To our knowledge, it also represents the first time that two ground-based tropospheric ozone lidar systems have been compared at the same ground site within the United States.

2. Instrument descriptions

Each instrument's specific transmitter and receiver components are listed in Table 1. Several important differences between the two lidars systems are that the TROPOZ transmitter produces a much more energetic pulse (12–16 mJ) at a lower repetition rate (50 Hz) and range resolution (15 m) than the LMOL system. This enables the TROPOZ to resolve more of the free troposphere, and it can routinely retrieve ozone profiles at or above the tropopause height. Conversely, the LMOL transmitter has a much higher repetition rate (1000 Hz), a lower pulse energy (50 μJ), and a higher range resolution (7.5 m), which may help resolve ozone features on a shorter time scale in future scientific investigations.

a. GSFC TROPOZ DIAL

The ground-based GSFC TROPOZ DIAL has been routinely taking measurements in the Baltimore–Washington D.C. region (Greenbelt, Maryland; 38.99°N, 76.84°W; 57 m MSL) since fall of 2013, which is described in depth in Sullivan et al. (2014). The TROPOZ has been designed and installed in a 13-m transportable trailer. As compared to traditional stationary laboratories, lidar systems have shown comparable results in mobile units and have the advantage of being transportable (McGee et al. 1991).

The transmitter for the system is a spectra physics quanta-ray pulsed Nd:YAG laser that has two independent parallel laser cavities that have been optimized for

the conversion of the fundamental to the fourth harmonic at a wavelength of 266 nm at a repetition rate of 50 Hz. The beams pass through converging lenses, which focus each beam waist near the center of a 1.8-m-long Raman tube filled with hydrogen or deuterium (Haner and McDermid 1990). Helium (He) was introduced in the Raman tube in order to yield the highest possible Raman conversion of pump photons into first Stokes shift photons. The TROPOZ final pressure combination to generate 289 nm was 21 bar D_2/28 bar He and 14 bar H_2/42 bar He to generate 299 nm (Sullivan et al. 2014). The typical transmitted energies for the TROPOZ measurements are 12 (299 nm) and 16 (289 nm) mJ per pulse.

The receiver for the TROPOZ is a large 45-cm-diameter Newtonian telescope for detecting 289/299 nm at higher altitudes in the free troposphere and four smaller 2.5-cm refracting telescopes to obtain a signal near the surface for 289/299 nm. For the 45-cm telescope, the lidar return is focused at a field stop to produce a 1.0-mrad field of view (FOV). After the field stop, all ambient and laser light is reflected or transmitted using optical elements, such as beam splitters and interference filters, to ensure each photomultiplier tube (PMT) is only receiving the proper spectral signal. The 2.5-cm telescopes have a much wider FOV, 10.0 mrad, for the measurement of near-field signals. In each of the channels, narrowband [<1.2 nm full width at half maximum (FWHM)] interference filters are implemented to decrease the amount of ambient solar light. This improves the signal-to-noise ratio (SNR) in order to achieve ozone retrievals to upward of 12 km AGL during daytime hours.

The near-field signal can be difficult to detect because the outgoing beam's location and divergence, with respect to the telescope geometry, may limit complete beam detection. Once the entire beam has been confidently detected, it is necessary, particularly in the near-field channels, to reduce the magnitude of the return signals to a regime where saturation effects are correctable. To achieve this, neutral density filters are placed in front of the detectors to reduce the large signal strengths that can cause nonlinear saturation effects in the detector system. Once these saturation effects are eliminated, the higher signal (near field) channels can be joined to the lower signal (far field) channels to increase the dynamic range of the overall lidar system.

To further help prevention of saturation effects associated with the detector photocathode, the individual PMTs have been constructed with electronic gating capabilities. The electronic gates are set at specific altitudes in order to restrict known saturated signals from ever making it downstream into the data acquisition system. Individual photons are then counted by a transient recorder (Licel transient recorder 20–80) at a maximum counting rate of 250 MHz. The data acquisition process is controlled by LabView software and a real-time display of ozone concentrations is available during observations.

b. *Langley Mobile Ozone Lidar*

The ground-based LMOL has been routinely taking measurements in the Hampton Roads region (Hampton; 37.1°N, 76.39°W; 4 m MSL) since fall of 2013 and is described in Fromzel et al. (2010) and Pliutau and De Young (2013). This compact DIAL system was developed through the NASA Small Business Innovation Research (SBIR) program to provide ozone, aerosol, and cloud atmospheric measurements, and has been constructed and deployed in a mobile trailer for ground-based campaigns.

The laser transmitter consists of a Coherent, Inc., Evolution-30 TEM00 1-kHz diode-pumped Q-switched Nd:YLF laser pumping a Ce:LiCAF tunable UV laser with all the associated power and lidar control support units on a single-system rack. Following harmonic conversion of the 527-nm pump beam into the 263-nm fourth harmonic by the CLBO crystal, dispersive prisms are used to separate the 527-nm beam from the 263-nm pump beam. The 527-nm visible beam may be transmitted into the atmosphere for aerosol measurements, but it was not operational during this intercomparison.

The 263-nm beam is split by a beamsplitter into two pump beams that pump each face of the Ce:LiCAF crystal. A short laser cavity consisting of a 60% reflective (1-m radius of curvature) output mirror, a dispersive prism, and a flat oscillating highly reflecting (HR) mirror is used to produce UV wavelengths, selectable between 282 and 310 nm. The wavelengths used during this intercomparison period were 287.09 and 292.7 nm.

The lidar receiver system consists of a telescope with a 40-cm-diameter parabolic mirror with a 1.4-mrad FOV. A fiber-optic cable with a 1-mm core diameter transmits the received signal from the telescope to the receiver box, which houses the detectors. The lidar control software is a National Instrument Lab Windows–based package that allows a graphical user interface for easy operation of menu-driven controls to configure the lidar. The software includes a program for real-time display of the ozone signals and for display of the ozone concentration calculated from atmospheric measurements.

c. *ECC sondes*

The most common method for validation of ozone lidars is sending balloonborne ECC instruments through

the atmosphere. Six Droplet Measurement Technologies (DMT/EN-SCI; model 2Z-V7; 0.5% buffer solution; Deshler et al. 2008), standard NOAA pressure-dependent flow-rate correction applied (Johnson et al. 2002) ozonesondes, coupled with InterMet (iMet) rawinsondes (iMet-1-RS), were flown throughout the campaign period to provide adequate sampling of the diurnal variability of the ozone column. Sonde ascent rates were varied throughout the campaign to improve vertical profile resolution. Preflight sonde conditioning routines were followed as specified in the Global Atmosphere Watch (GAW) report (Smit and ASOPOS Panel 2011) in accordance with community standard practices. The ECC sondes used in this intercomparison typically yield a precision better than ±(3–5)% and an accuracy of about ±(5–10)% (Smit et al. 2007).

Persistent westerly winds blew all sondes over the Chesapeake Bay, toward the Chesapeake Bay Bridge Tunnel (CBBT, approximately 15–20 km east of LaRC) connecting Hampton Roads to the Eastern Shore. Each of the sondes flew over land for the first 10 min (approximately 3000 m) and over the Chesapeake Bay for the remainder of the trajectory. An unusual phenomenon was observed during all flights, in that all data transmission ceased just before the sondes crossed the CBBT regardless of altitude. The cause of this interruption is unknown, but it may be due to temporary heavy radio traffic to the east and/or military exercises in the Atlantic Ocean.

3. Raw signal analysis

Before the retrieval of ozone can be completed, it is important to analyze the quality of the raw signals that are being collected during the observation times. Figure 2 shows the natural log of the range-corrected raw signals for the LMOL and TROPOZ DIAL instruments. The range-corrected signals are approximately linear for a homogeneous atmosphere and deviations from the linearity likely indicate regions of potential saturation, misalignment, or incomplete telescope overlap. These 10-min averages from each instrument's data acquisition system are from 0400 to 0410 UTC 4 May 2014. The times were chosen because they represent the typical temporal averaging time of each system. The raw signals were chosen from a time following nautical twilight, when each system achieves the best SNR because of negligible solar background radiation.

The top panel of Fig. 2 shows the analog (AN) and photon-counting (PC) signals from the LMOL for each of the wavelengths (292–292.70, 287–287.09 nm). The photon-counting signals above 2 km MSL, aside from small deviations near 3.2 km MSL, are mostly linear, indicating a homogenous and near-Rayleigh atmosphere. This feature near 3.2 km MSL corresponds to the presence of clouds. At altitudes below 1.5 km MSL, the deviation from the linearity in the photon-counting signals can be ascribed to incomplete overlap or detector saturation effects. The analog detection signals are also mostly linear; however, the signals may exhibit an incomplete overlap or beam misalignment at altitudes below 0.4 km MSL. During the observation, the LMOL data acquisition system was configured to record only the first 1200 bins at 7.5-m widths, resulting in a maximum possible altitude of 7600 m because the first 74 bins (555 m) are before the laser trigger pulse and the last 10% of data points are removed in the linear background subtraction. This method limits the upper altitudes of the retrieval; however, it does ensure that the solar background contamination is removed from the system. Although the data registration record was limited for this intercomparison, it has been doubled for future observations to ensure that the return signals extend out to a region where they are indiscernible from the solar background radiation.

The TROPOZ signals (289 and 299 nm) are shown in the bottom panel of Fig. 2, and the abbreviations are for the 2.5-cm near-field receivers (MI) and the larger 40-cm main telescope (MA) at the near field (LO) and far field (HI). Similar to LMOL photon-counting channels, the TROPOZ signals are all mostly linear besides the small deviation near 3.2 km MSL. All of the signals will require a correction due to saturation effects at the lowest altitudes of each profile. However, the use of multiple telescopes provides an extensive altitude range coverage between the profile merge regions to minimize potential overlap and saturation effects. A slope change in the 289 MAHI channel (MAHI 289) is observed near 10 km MSL, which coincides with the increased absorption in signal from ozone associated with the tropopause. As the photon-counting signal strengths diminish and approach a slope of zero, as in the MAHI 289 signal above 14 km MSL, the usable laser light is nearing the ambient background light levels. At this altitude, the signal-to-noise ratio begins to largely affect the signal and limit the upper-altitude extent of the retrieval.

Each of these systems has been transported prior to this intercomparison study to confirm the mobility of the systems. Although some optical realignment is necessary after transport, the systems are able to be quickly optimized for atmospheric observations.

4. The DIAL equation

It is possible to write the DIAL equation (Megie et al. 1985) in terms of the range bins specified as

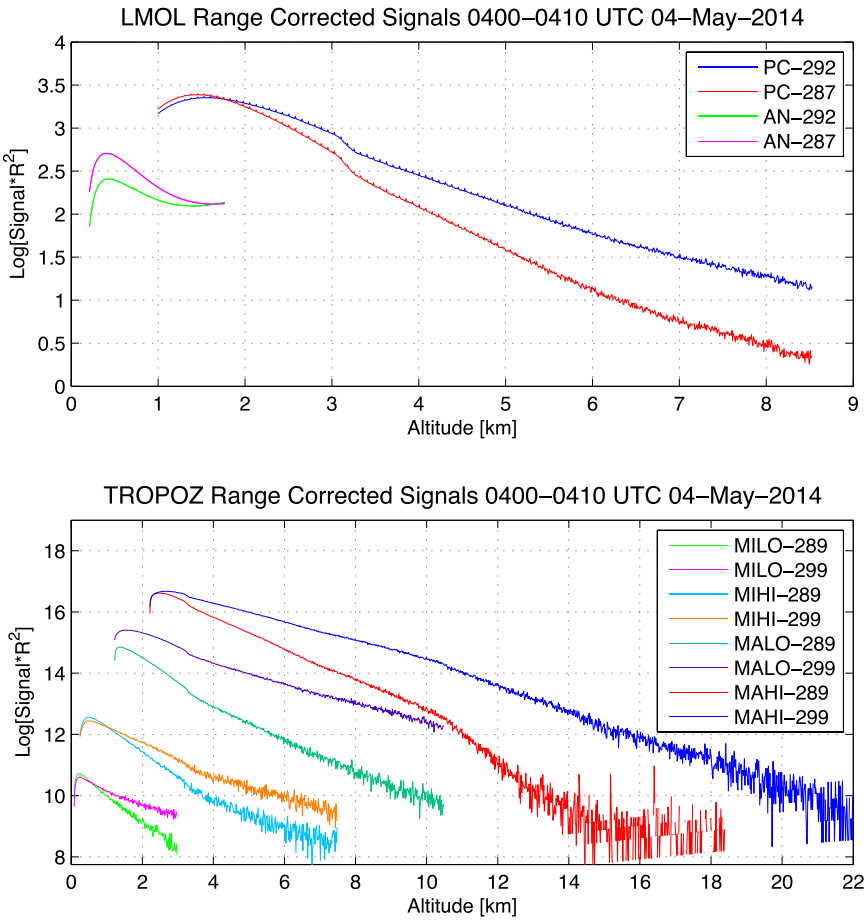

FIG. 2. The range-adjusted raw signals from both the (top) LMOL and (bottom) TROPOZ. The abbreviations are for photon counting (PC) and analog (AN) detection at the respective wavelengths. The TROPOZ abbreviations, which are photon counting only, are for the return signals detected by the small near field receivers (MI) and the large main telescope (MA) at the upper (HI) and lower (LO) altitude ranges.

$$N_{O_3}(r) = \frac{1}{2\Delta\sigma_{O_3}} \frac{d}{dr}\left\{\ln\left[\frac{P_{\text{off}}(r)}{P_{\text{on}}(r)}\right] - \ln C\right\} - D, \quad (1)$$

where

$$C = \frac{\beta_{\text{off}}(r)}{\beta_{\text{on}}(r)}, \quad (2)$$

where $\beta = \beta_{\text{mol}} + \beta_{\text{aer}}$, and

$$D = \frac{\Delta\alpha_{\text{mol}}}{\Delta\sigma_{O_3}} + \frac{\Delta\alpha_{\text{aer}}}{\Delta\sigma_{O_3}} + \sum_i \frac{N_{\text{IG}_i}\Delta\alpha_{\text{IG}_i}}{\Delta\sigma_{O_3}}. \quad (3)$$

For these equations, N_{O_3} is the ozone number density and $\Delta\sigma_{O_3}$ ($\sigma_{\text{on}} - \sigma_{\text{off}}$) is the difference in corresponding ozone absorption cross sections taken at the two DIAL wavelengths. The optical power returned to the receiver, atmospheric backscatter coefficient, and atmospheric extinction coefficient, at range r at either the "on" or "off" wavelength, are denoted as P, β, and α respectively. The $\Delta\alpha$ ($\sigma_{\text{on}} - \sigma_{\text{off}}$) in (3) is composed of the differences between the two DIAL wavelengths in the extinction coefficient for Rayleigh (or molecular, denoted as mol) scattering, aerosol (aer) scattering, and absorption by other interfering gases (IG).

The terms (2) and (3) correspond to the differential Rayleigh and aerosol backscatter at the "on" and "off" wavelengths. Because the spectral dependence of aerosol scattering and extinction are not known exactly, the differential aerosol extinction [second term in (3)] was determined using the iterative technique described in Sullivan et al. (2014), which found corrections throughout the PBL of mostly <3 ppbv (or <5%) for the observation period. It is known that aerosol gradients can cause a significant error in the ozone retrieval (Browell et al.

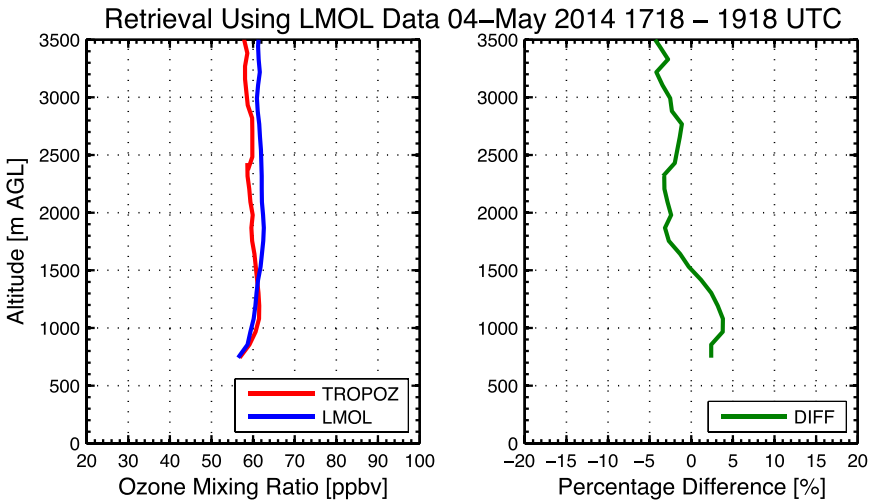

FIG. 3. (left) A comparison between the LaRC and GSFC retrieval algorithms with identical input data and vertical resolution. (right) The relative ozone percentage difference between the two retrievals.

1985); however, strong westerly winds cleared out a majority of local pollutants during the observation period and thus aerosol gradients were likely small. The Aerosol Robotic Network (AERONET; Holben et al. 1998) sun photometer measurement located at NASA LaRC during the observation period retrieved a mean aerosol optical depth (AOD; at 500 nm) of 0.23, which is indicative of clean continental air (Mulcahy et al. 2009). To emphasize the absence of aerosols during the observation period, the May 2014 monthly mean AOD (at 500 nm) at NASA LaRC was nearly 4 times larger, with a value of 0.844. Also during the observation period, interfering gases, such as large concentrations of SO_2 and NO_2, were assumed to be negligible.

5. Algorithm intercomparison

a. Algorithm comparison using identical data

Before retrieving and comparing the final ozone product, it was important to confirm that each group's retrieval algorithm could return a similar result when using the same vertical resolution and identical input data to within a reasonable percentage difference (±5%). Analyzing the same dataset with the same spectral parameters, such as the Rayleigh molecular correction, ensures that any biases found in the intercomparison are limited to those parts of the algorithms that do not pertain to parameter choice. This analysis used a 120-min (1718–1918 UTC 4 May 2014) average of the LMOL analog signals. This time period was chosen because it had an appreciable amount of solar background radiation that required a correction and the temporal average was chosen in order to minimize potential statistical uncertainty differences resulting from the use of different smoothing schemes.

The left panel of Fig. 3 shows the retrieved ozone mixing ratio profile from the TROPOZ DIAL and the LMOL algorithms. The meteorological variables for this analysis were taken from the sonde that was launched at 1901 UTC 4 May 2014. The two algorithms use the same linear background subtraction region (trailing 10%). The differential ozone absorption cross section used was $9.677 \times 10^{-23}\,\mathrm{m}^2$ (Malicet et al. 1995) with no temperature dependence. The Rayleigh extinction was derived from the number density of air derived from the sonde and the differential Rayleigh molecular extinction cross section used for the analysis was $5.515 \times 10^{-31}\,\mathrm{m}^2$ (Measures 1984).

For this comparison, computation of the derivatives is done using the discrete data. The LMOL retrieval implements a finite numerical difference approximation and uses 90-m block averages and a five-point least squares smoothing technique. The TROPOZ retrieval utilizes a second-order Savitsky–Golay (SG) differentiation filter (Savitzky and Golay 1964) with a fixed window width of 27 bins to perform the derivative and smoothing during one step. Both retrievals yield the same vertical resolution of 225 m, which are defined by the FWHM of the coefficients of the least squares or SG smoothing filters. The block averaging and smoothing as compared to the SG smoothing filter appears to smooth out finescale features and variability that may be important to preserve at finer temporal resolutions.

The right panel of Fig. 3 shows the relative ozone percentage difference between the two algorithms. The

relative percentage difference used throughout this paper has been calculated as

$$\Delta N_{O_3}(\%) = \frac{\mathrm{TROPOZ}_{N_{O_3}} - \mathrm{LMOL}_{N_{O_3}}}{\mathrm{TROPOZ}_{N_{O_3}}} \times 100, \quad (4)$$

where $\mathrm{TROPOZ}_{N_{O_3}}$ has been chosen as the reference retrieval for the comparison. This shows agreement within ±5% of each other between 750 and 3500 m. The differences can be mainly attributed to the different derivative and smoothing techniques employed, and the agreement is close enough to assume that the individual algorithms yield nearly identical ozone profiles.

b. *Final algorithm specifications*

The final LMOL retrieval algorithm used throughout the remainder of this paper is similar to the retrieval described in the previous section, except the smoothing scheme is altered to achieve better agreement at higher altitudes. The analog detection retrieval uses 90-m (12 bins) block averages and a five-point least squares smoothing technique, and the photon-counting retrieval uses 112.5-m (15 bins) block averages and a nine-point least squares smoothing. The vertical resolutions, which are defined by the FWHM of the coefficients of the least squares smoothing, are 225 and 506.25 m, respectively. The retrieved ozone profiles are then merged to form one continuous ozone profile.

The final TROPOZ retrieval algorithm used throughout the remainder of this paper is modified from that described in Sullivan et al. (2015). The background due to ambient light was determined where the background signal was a constant at altitudes above 30 km. Because the TROPOZ has eight separate PMTs, the retrieval algorithm implements eight different dead time (pulse pileup) corrections with values between 4.3 and 6 ns due to a different signal saturation effect in each detector (Lampton and Bixler 1985). Typically, the near-field MILO and MIHI channels (with larger FOV) are more susceptible to saturation effects during the enhanced daytime solar background radiation and therefore use a larger dead time correction, while the MALO and MAHI are mostly between 4.3 and 5 ns. The finite impulse response (FIR) SG differentiation filter has been used to produce the required first-order derivative. Atmospheric profiles of temperature and number density are then implemented from standard model or sonde launches to produce the most accurate retrieval.

Similar to the LMOL retrieval, a final continuous profile is merged between multiple channels and the final vertical resolution of the data is determined using the FWHM of the steady-state filter coefficients associated with the smoothing filter window size. Figure 4 shows the difference in vertical resolution between the two algorithms. Because increasing statistical uncertainties are more likely to cause a bias from the decrease in the signal-to-noise ratio with altitude, it is favorable to increase the number of points of the derivative low-pass filter used for data processing (Godin et al. 1999). This allows for near-surface data to be minimally smoothed and the higher-altitude measurements, which are typically less dynamic, to be smoothed over greater altitude ranges.

6. Retrieval intercomparison analysis

After the algorithms were analyzed for congruence during an optimal case, it was necessary to investigate the performance of each system's algorithm on its respective data at a finer temporal resolution and to compare it to a reference profile. The final ozone mixing ratios are presented as compared to the six independent ECC sonde launches during the time series from 0400 to 1918 UTC 4 May 2014. A comparison is presented of the entire time series of data, which shows how each instrument can represent the evolving nature of ozone within the PBL and free troposphere and where explainable differences have occurred. There is also a discussion of the TROPOZ retrieval with its full range and resolution. The ozone column average, within the observed range, is shown as a direct comparison to the ECC sondes. The section concludes with a statistical comparison of the retrievals.

a. *Individual ozone profiles compared to ECC sondes*

Figure 5 shows the TROPOZ and LMOL ozone profiles as compared to six ECC sondes in the retrieved range below 7500 m. The sonde launch times are noted above each plot. The lidar profiles are temporal averages of the data over the 10-min segment following each sonde launch, and both retrievals have utilized the sonde meteorological data to achieve the most accurate retrieval. Loss of telemetry in the ozonesondes accounts for the white space above 4500 m in the last two sonde comparisons. The small gaps at 0415 and 1348 UTC are also due to telemetry issues, but the sondes eventually reached a location where they could continue transmission. Additionally, clouds moved into the region during the 0646 UTC sonde launch and LMOL data between 2750 and 3750 m AGL have been removed because of increased noise in the retrieval.

All of the panels in Fig. 5 show good agreement between the lidars and the sondes. The first three panels

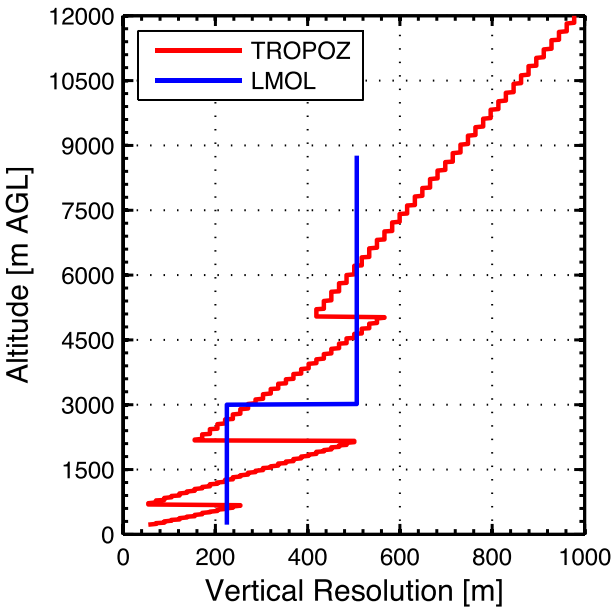

FIG. 4. The vertical resolutions for each system used in the retrieval intercomparison. The LMOL retrieval uses a different constant block averaging for the AN and PC regions, whereas the TROPOZ retrieval implements a variable vertical resolution scheme throughout the entire retrieved atmosphere.

correspond to the nighttime portion of the observation period, in which the SNR of each system was the highest and the retrieval is extended to higher altitudes. As the solar background radiation increases, it is more difficult, particularly for the LMOL system, to accurately resolve upper-altitude ozone concentrations.

The uncertainty bars in Fig. 5 represent the full uncertainty in each instrument, and the largest contribution comes from the statistical uncertainties associated with photon counting and analog detection through the use of PMTs (Papayannis et al. 1990). During this observation period and for the retrieval range below 4500 m, the statistical uncertainties ranged from 4% to 11% for the TROPOZ and from 3% to 13% for the LMOL. Although aerosols may cause a significant uncertainty in the final retrieval (Browell et al. 1985), due to the rather unpolluted atmospheric conditions described previously, a correction in the retrieval due to aerosols within the PBL has been quantified as ≤5%, which is comparable to or less than the statistical uncertainty of the measurements. A full description of the TROPOZ retrieval uncertainty analysis, which the LMOL uncertainty analysis is based on, can be found in Sullivan et al. (2014, 2015). Overall, this figure is meaningful because it indicates that each of the sonde profiles falls mostly within the uncertainty bars of each of the retrievals and confirms that no large biases, particularly from aerosols, are apparent.

Figure 6 shows the relative differences between the TROPOZ (red) and LMOL (blue) retrievals and each ozonesonde in relative percentage in the retrieved range below 7500 m. The TROPOZ retrieval is within ±25% of the sonde throughout the entire observation period. The LMOL retrieval is within ±25% for most of this altitude range, especially in the first three plots where the SNR is adequate for a larger range. The LMOL retrieval is not utilizing the temperature dependence of the ozone absorption cross sections, which may add in a small difference in the final comparison profile. As mentioned earlier, persistent westerly winds blew all sondes directly over the Chesapeake Bay and this separation distance may be a reason for observed atmospheric differences.

It was important to summarize the findings from Fig. 6 and state how each of the lidar retrievals directly compared to all of the ozonesondes. Figure 7 shows the mean relative differences of retrieved ozone mixing ratios between all of the ozonesondes and each of the lidars. Profiles are presented for the TROPOZ (top panel) and LMOL (bottom panel), and the green lines represent two standard deviations of the mean relative differences. Overall, the TROPOZ retrieval is mostly within ±10% below 7500 m and the TROPOZ standard deviation profiles are mostly within ±20% for the retrieval below 6000 m. Because the zero line falls within two standard deviations of the relative differences, there is no significant systematic bias present in the TROPOZ measurement as compared to the ozonesondes. The LMOL retrieval is also mostly within ±10% in the retrieved region below 4500 m. Above this altitude, the mean differences relative to the ozonesonde are near 20% due to decreasing SNR and increasing statistical uncertainties. However, in the retrieved region below 4500 m, the zero line falls within two standard deviations of the relative differences and there is no significant systematic bias present in the LMOL measurement.

b. *Ozone time series and relative differences between retrievals*

Although the comparison of individual ozone profiles with appropriate reference profiles are helpful in determining specific retrieval differences, it is important to analyze the entire continuous lidar time series to understand how each retrieval characterizes the evolution of the ozone throughout the PBL and free troposphere. This also emphasizes the utility of the ozone lidar as an ozone monitor, which yields much more valuable and detailed information about the time evolution of the ozone profile than the series of ECC sondes launched during the intercomparison. Figure 8 shows the TROPOZ retrieval (top panel), LMOL retrieval (middle panel), and the

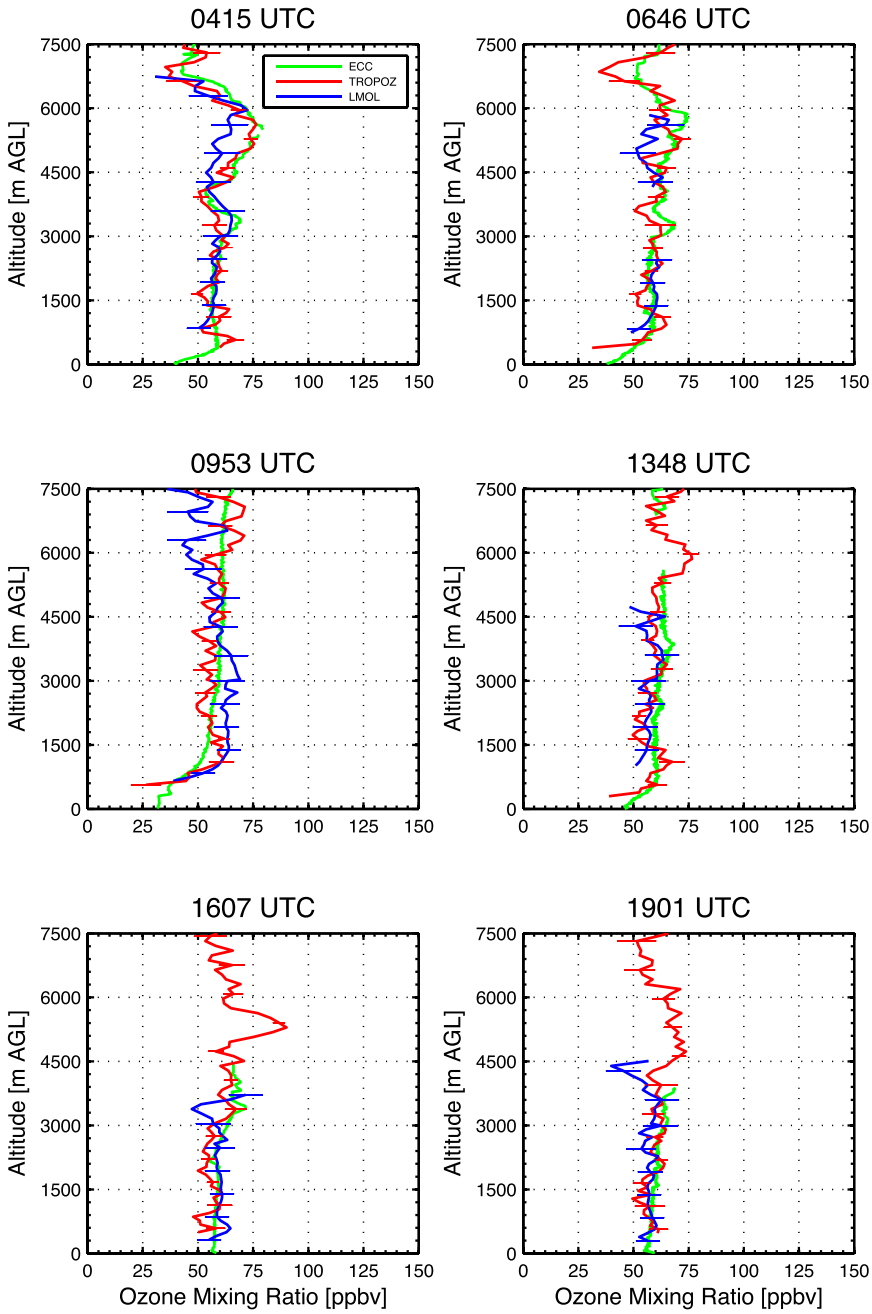

FIG. 5. Six individual ozone profiles from the TROPOZ and LMOL algorithms as compared to each ozonesonde during the observation period 0400–1918 UTC 4 May 2014.

relative percentage difference between the two retrievals (bottom panel). All of the ECC sonde profiles are overlaid on the lidar time series plots at the launch times and are marked with red triangles along the time axis. Neither of the last two sondes achieved altitudes above 4.5 km. There was a thin cloud layer from 2750 to 3750 m between 0430 and 1000 UTC, and this region has been blocked out in the plots.

From the TROPOZ retrieval, it is possible to see the presence of a 60–80-ppbv ozone layer in the region from 4500 to 6000 m in the beginning of the observation period. A region of higher ozone concentrations, 90–100 ppbv, subsides into the observation range near 0900 UTC. A 70–80-ppbv plume of ozone also exists, which is centered around 4500 m from 1130 to 1330 UTC. Overall, the TROPOZ retrieval shows good

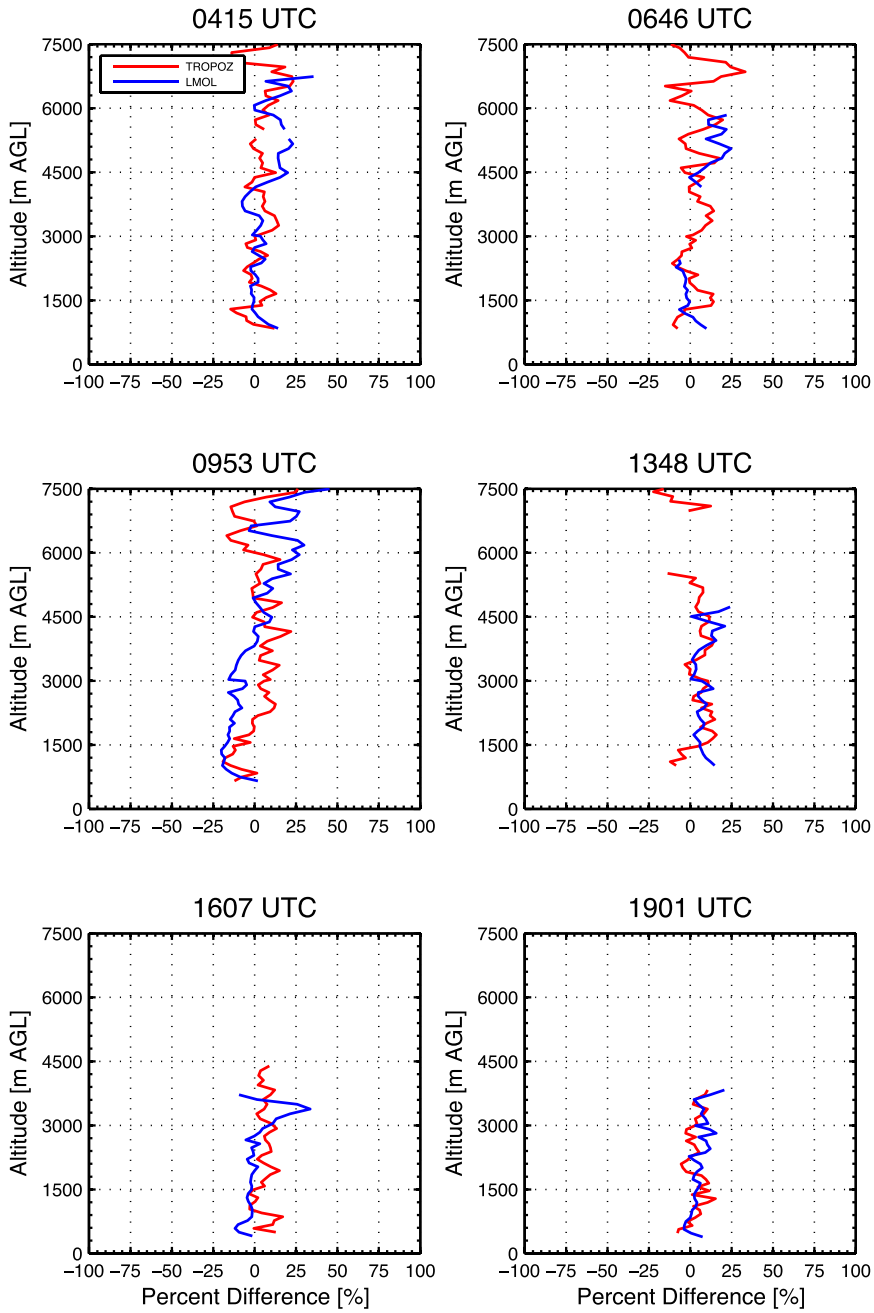

FIG. 6. Relative percentage ozone differences from the TROPOZ and LMOL algorithms as compared to each ozonesonde during the observation period 0400–1918 UTC 4 May 2014.

agreement with the ECC sondes and especially at 0415 and 0646 UTC, where the ECC profiles also resolve the ozone feature between 4500 and 6000 m near the beginning of the observation period. The TROPOZ retrieval algorithm currently reports ozone mixing ratios up to 12 000–14 000 m, but only data up to 7750 m are shown in Fig. 8 for the purpose of comparison with the LMOL retrieval. Later on, Fig. 9 will show the TROPOZ data over its full altitude range. There, a more complete picture of the evolution of the aloft ozone layers can be seen, including the observation of ozone subsiding from the region of the tropopause into the free troposphere.

The LMOL retrieval also picks up the lower portion of the 70–80-ppbv ozone plume centered at 4500 m from 1130 to 0130 UTC that was previously discussed. The LMOL-retrieved ozone concentrations match well with

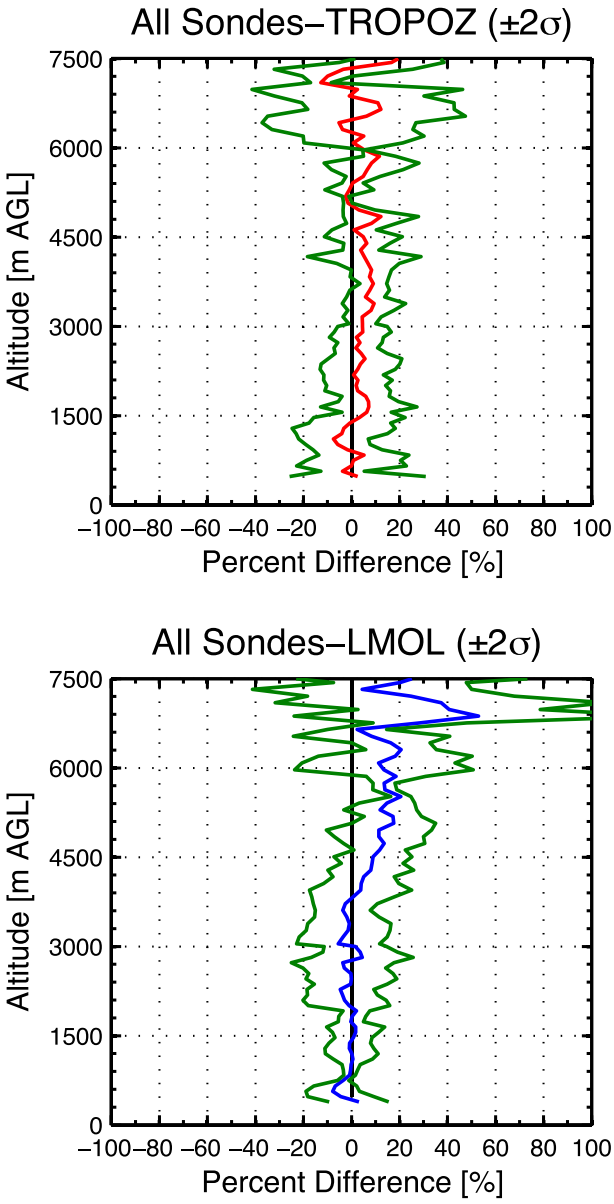

FIG. 7. Mean relative percentage differences between all of the ECC sondes and the retrieved ozone mixing ratios from the (top) TROPOZ and (bottom) LMOL. The green lines represent two standard deviations of the mean relative differences.

the ozonesondes in the region of adequate SNR, especially at 1348 UTC. From 0800 to 1030 UTC in the region below 3000 m, the LMOL retrieval indicates higher values than the ozonesonde launched at 0946 UTC. This suggests that there was likely additional cloud contamination in the LMOL retrieval during this time. A discontinuity occurred in the LMOL time series near 1520 UTC, when the transmitted laser beam was realigned to the telescope to increase the SNR in the near field. After the beam realignment, the ozone concentrations are much closer to the ECC sonde. However, an increase in ozone concentrations from 1700 to 1900 UTC below 2000 m exists, which may be due to unintentional beam drift. Although this occurred, the realigned portion of the LMOL retrieval, even down near 500 m, shows good agreement with the ECC sonde at 1901 UTC, which is encouraging for future scientific investigations and field campaigns.

The bottom panel of Fig. 8 shows the time series chart for the relative percentage difference, from (4), between the two ozone lidars. There is agreement to within ±10% throughout most of the PBL and lower free troposphere in the observable region. Positive biases occur in the upper-altitude region, where the SNR is minimal in the LMOL retrieval. Biases also exist in the regions where the LMOL reports higher ozone concentrations near clouds and after the LMOL beam realignment, which were discussed above.

c. *GSFC TROPOZ DIAL retrieval for full observation range*

The analysis of the TROPOZ time series data shown in Fig. 8 does not depict the full capabilities of the instrument and retrieval, which are better illustrated in Fig. 9. The TROPOZ can routinely retrieve ozone concentrations to altitudes near 14 000 m during the nighttime hours and 12 000 m during daylight hours. This emphasizes the ability to characterize the temporal evolution of ozone laminas throughout the free troposphere and the interaction with the tropopause, which has previously resulted in the characterization of a stratospheric–tropospheric exchange (STE) event of ozone in the Baltimore–Washington, D.C., region (Sullivan et al. 2014).

The retrieval shows good agreement with the ECC sondes, especially at 0415 and 0646 UTC, where the sondes validate the TROPOZ-retrieved profiles in the range between 4500 and 11 000 m. By restricting the analysis to the first 7000 m of the time series, it is difficult to understand the sources of evolving ozone laminas. With the full TROPOZ retrieval, it can be observed that enhanced ozone below the tropopause existed and most likely subsided in the troposphere due to dynamics in the region near the tropopause.

At the beginning of the observation period, an ozone feature was present between 4500 and 6000 m, with concentrations between 60 and 80 ppbv, and a region of comparably lower ozone concentrations, between 40 and 60 ppbv, from 6000 to 8000 m. A nearly 20-ppbv gradient in ozone between these layers near 6000 m was verified by the ozonesondes at 0415 and 0646 UTC.

Another interesting ozone feature during the observation period was the appearance of a 100–150-ppbv

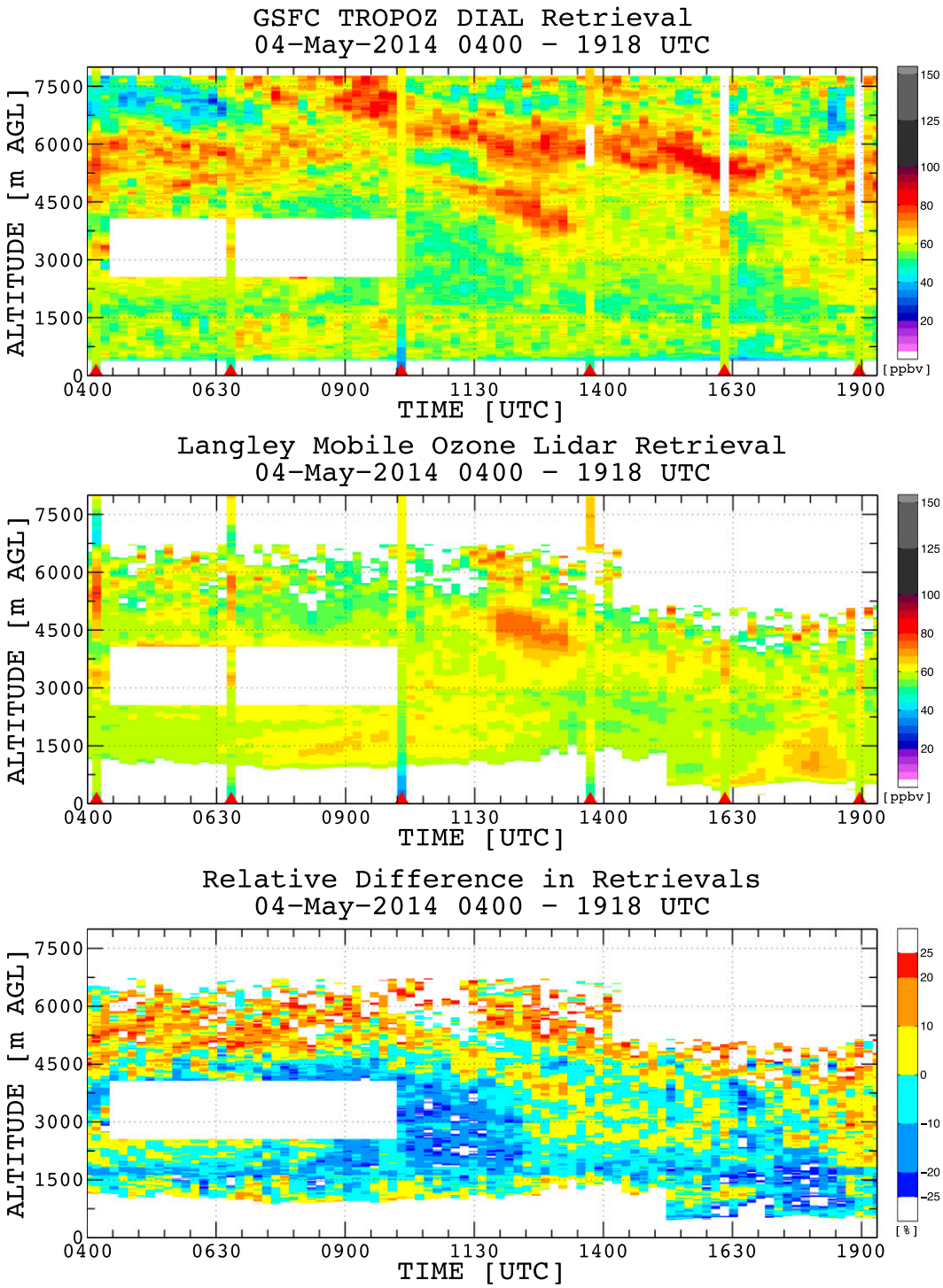

FIG. 8. (top) The TROPOZ retrieval, (middle) LMOL retrieval, and (bottom) the percent difference between each of the retrievals. The ozonesondes are denoted by a red triangle at the launch time. White spaces in the retrievals are due to cloud contamination or inadequate signal. White space in the ozonesonde profiles are due to loss of data in the sonde telemetry.

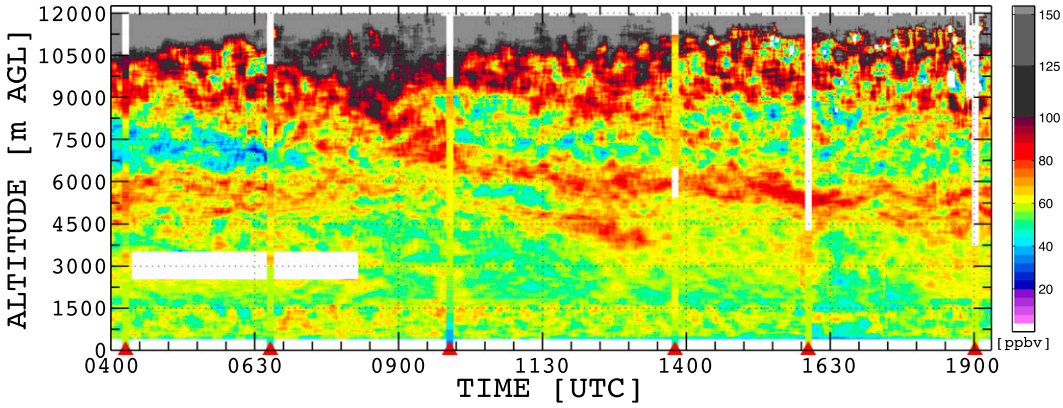

FIG. 9. The TROPOZ algorithm from 375 to 12 000 m. With the full TROPOZ retrieval, it can be observed that there was residual ozone aloft that existed before observations began. Additional ozone was also present that most likely subsided due to dynamics in the region near the tropopause.

ozone reservoir subsiding from the tropopause near 0700 UTC, which mixed down into the upper free troposphere with ozone concentrations between 90 and 100 ppbv throughout the remainder of the observation period. Evidence of this ozone originating in the stratosphere is provided in the meteorological data from the ECC sonde at 0646 UTC. These data (not shown) reveal that this region of high ozone below the tropopause (7500–9500 m) had a decrease in relative humidity (ΔRH = −30%) and temperature ($\Delta T = -5$ K), which are indicators of an air mass originating in the stratosphere (Danielsen 1968).

d. Observed column averages

The TROPOZ and LMOL systems are intended to provide data that can be of use to the air quality community, particularly in the form of a product that can be readily integrated into air quality models. One such product is the average ozone mixing ratio value, at a given time, over some specified altitude range. For convenience, we shall refer to this product as the observable ozone column average, not to be confused with an integrated column ozone value. To calculate this product for the intercomparison described in this paper, we have chosen to use a temporal resolution of 10 min and an altitude range from 1000 to 4500 m. This altitude range covers the region where each of the lidars has good alignment, is not affected by signal saturation, and has reasonable statistical uncertainties. The region with the cloud, including the region where the block averaging used by LMOL affected the retrieval, was excluded from the average calculation.

This product has been calculated for the two lidars and for the ECC sondes over the period of simultaneous measurement, and is shown in Fig. 10. The relative percentage differences between the lidars and the ECC sondes have also been calculated and are at the bottom of the figure. Overall, the lidars and sondes are in very good agreement for the observation period, with differences compared to the TROPOZ ranging from −2% to 4% with an average of −1.7% and LMOL ranging from −7% to 8% with an average of −3.1%. During the period of 0800–1230 UTC, the LMOL appears to have retrieved slightly higher average ozone mixing ratio values than those for the TROPOZ and ECC sonde. It was suggested in a previous discussion that this bias was likely due to cloud contamination, which can also be inferred from the curtain plots in Fig. 8 and the comparison plot for the 953 UTC sonde in Fig. 5.

The curtain plots in Fig. 8 also show that from 1100 to 1330 UTC an ozone layer descended into the region of the averaging column, which has affected both lidar averages. Other than these features, the ozone column average remains fairly uniform during the observation, varying slightly around the value of 60 ppbv, which can be taken as an estimate of the background ozone mixing value. Overall, the percent differences between the observed column average and the ECC sondes are within ±8%, which is evidence that each of these instruments is able to support the air quality community with accurate ozone observations.

e. Bias between retrievals

It is important to seek any information on systematic biases in the retrieval of the lidar products. In addition to the difference plots already discussed, we have performed an analysis using a Bland–Altman plot. In what follows, we have placed limits on the region of data to be considered. As previously shown, the LMOL retrieval suffered from a misalignment of its transmitted beam and telescope. This affected the retrieval below 1000 m and this region has been excluded from consideration

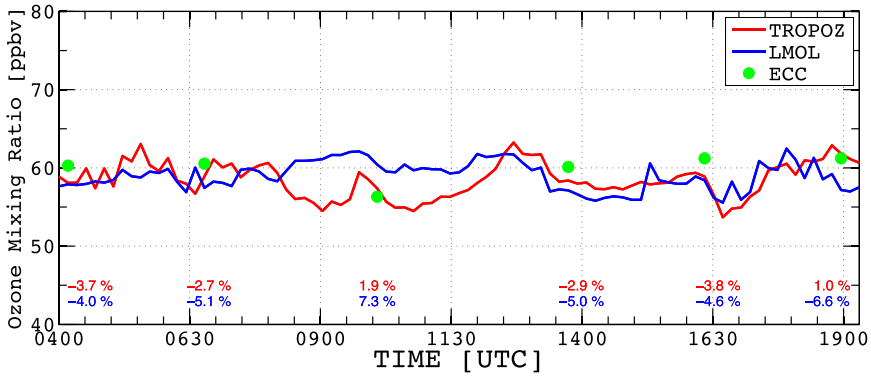

FIG. 10. Comparison of the column averages for ozone concentrations between the TROPOZ, LMOL, and ECC sondes for the range between 1000 and 4500 m. The percent differences between the lidars and the ECC sondes are shown at the bottom of the figure.

here. Also, the SNR of the LMOL deteriorated above 4500 m during the day and data above this altitude have also been excluded. Regions of cloud interference have also been excluded. To make correlation calculations, this data region was divided into cells with a 10-min width and a 90-m height. The choice of a 90-m height was necessary, as the LMOL data were presented using a 90-m block average and the TROPOZ data were averaged accordingly.

Bland–Altman plots are frequently used to evaluate the agreement between two different instruments or two measurement techniques. They are particularly useful in the task of identifying systematic differences and outlying data points (Bland and Altman 1999). Figure 11 shows the Bland–Altman plot for the TROPOZ and LMOL data over the region previously described for use in comparisons. The abscissa is the average and the ordinate is the difference of the retrieved ozone mixing ratio values for the two instruments. The green line in the figure is the mean of the differences. The black dashed lines mark the limits of agreement for 95% of all the data.

The mean difference for the comparison over the specified data region is calculated to be a value of −0.71 ppbv. This corresponds to a bias of ≤2% as compared to the measurement values throughout the observation period for the two instruments (see Fig. 10). The 95% limits of agreement occur at +5.53 and −6.96 ppbv. This can be restated to say that 95% of the simultaneous measurements (over altitude and time) differ from the approximate average retrieved value of 60 ppbv by some percentage between −11.6% and 9.2% (the sign being determined by the definition of the difference as the TROPOZ value minus the LMOL value). As the mean difference value is roughly 2% of the average retrieved value, and as the 95% limits of agreement are similar in magnitude to the statistical uncertainties of the retrieval products, it appears that there is no statistically significant bias.

To further investigate this conclusion, the mean and standard deviation of difference values for each 1-ppbv-wide bin of the average value (abscissa value in Fig. 11) have been calculated and plotted on the Bland–Altman plot. Here the red curve is drawn connecting the mean values and the red bars are the standard deviations of the distribution of difference values. It can be seen that both the mean difference value (green line) and the zero difference value fall within the standard deviation bars along most of the mean curve (red line). The sample populations in the abscissa bins near the ends of the mean curve are so small that we feel justified in excluding them. This further strengthens the assessment that there is no statistically significant systematic bias between the TROPOZ and LMOL instruments.

7. Conclusions

The intercomparison between the GSFC TROPOZ DIAL and LMOL was performed for 15 h on 4 May 2014 to validate the operation and retrieval products of these very different transportable systems for ozone science investigations within the troposphere. Six ozonesondes were launched during this time to provide reference ozone profiles. Retrieved ozone profiles have shown to be mostly within 10% of each other, as well as with the ozonesondes. The observed column averages as compared to the ozonesondes are also mostly within 8%. A robust uncertainty analysis indicates that the average mean difference between the lidar retrievals is less than 2% and that there is no statistically significant systematic bias between the TROPOZ DIAL and LMOL instruments.

The agreement of the 15-h-long observation, for each of the lidars over substantial altitude ranges (1000–6000 m at night and 1000–4500 m during daytime),

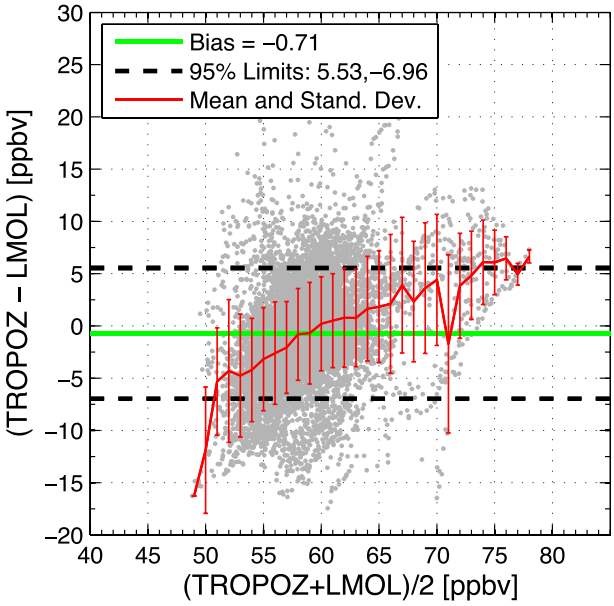

FIG. 11. The Bland–Altman plot for the TROPOZ and LMOL data over the region from 1000 to 4500 m.

demonstrates that these systems can accurately characterize the evolution of ozone in the PBL and free troposphere, where lidar SNR is sufficient. This was a critical experiment, as these two lidars are part of the Tropospheric Ozone Lidar Network (TOLNet) and their ozone profile data will be used to validate air quality model forecasts and tropospheric ozone retrievals from satellites. The authors believe that this intercomparison has significantly added to the confidence that both LMOL and TROPOZ are capable and useful instruments for monitoring tropospheric ozone in future atmospheric science campaigns. This is also, to the best of our knowledge, the first reported intercomparison between two ground-based tropospheric ozone lidars within the United States.

Acknowledgments. The authors gratefully acknowledge the support for this study provided by Jack Kaye (NASA HQ), the NASA Tropospheric Chemistry Program, the Tropospheric Ozone Lidar Network (TOLNet), the Maryland Department of the Environment (Contract U00P7201032), and the NOAA–CREST CCNY Foundation CREST Grant (Contract NA11SEC481004). Also, thanks to Raymond M. Hoff for providing extended discussions of lidar techniques.

REFERENCES

Bland, J. M., and D. G. Altman, 1999: Measuring agreement in method comparison studies. *Stat. Methods Med. Res.*, **8**, 135–160, doi:10.1177/096228029900800204.

Browell, E. V., S. Ismail, and S. T. Shipley, 1985: Ultraviolet DIAL measurements of O_3 profiles in regions of spatially inhomogeneous aerosols. *Appl. Opt.*, **24**, 2827–2836, doi:10.1364/AO.24.002827.

Danielsen, E. F., 1968: Stratospheric–tropospheric exchange based on radioactivity, ozone and potential vorticity. *J. Atmos. Sci.*, **25**, 502–518, doi:10.1175/1520-0469(1968)025<0502:STEBOR>2.0.CO;2.

Deshler, T., and Coauthors, 2008: Atmospheric comparison of electrochemical cell ozonesondes from different manufacturers, and with different cathode solution strengths: The balloon experiment on standards for ozonesondes. *J. Geophys. Res.*, **113**, D04307, doi:10.1029/2007JD008975.

Fromzel, V., C. Prasad, K. Petrosyan, Y. Liaw, M. Yakshin, W. Shi, and R. De Young, 2010: Tunable, narrow linewidth, high repetition frequency ce:LiCAF lasers pumped by the fourth harmonic of a diode-pumped Nd:YLF laser for ozone DIAL measurements. *Advances in Optical and Photonics Devices*, K. Y. Kim, Ed., INTECH, 101–116.

Godin, S., and Coauthors, 1999: Ozone differential absorption lidar algorithm intercomparison. *Appl. Opt.*, **38**, 6225–6236, doi:10.1364/AO.38.006225.

Haner, D., and I. McDermid, 1990: Stimulated Raman shifting of the Nd:YAG fourth harmonic (266 nm) in H_2, HD, and D_2. *IEEE J. Quantum Electron.*, **26**, 1292–1298, doi:10.1109/3.59670.

Holben, B., and Coauthors, 1998: AERONET—A federated instrument network and data archive for aerosol characterization. *Remote Sens. Environ.*, **66**, 1–16, doi:10.1016/S0034-4257(98)00031-5.

Johnson, B. J., S. J. Oltmans, H. Vömel, H. G. J. Smit, T. Deshler, and C. Kröger, 2002: Electrochemical concentration cell (ECC) ozonesonde pump efficiency measurements and tests on the sensitivity to ozone of buffered and unbuffered ECC sensor cathode solutions. *J. Geophys. Res.*, **107**, 4393, doi:10.1029/2001JD000557.

Lampton, M., and J. Bixler, 1985: Counting efficiency of systems having both paralyzable and nonparalyzable elements. *Rev. Sci. Instrum.*, **56**, 164–165, doi:10.1063/1.1138462.

Malicet, J., D. Daumont, J. Charbonnier, C. Parisse, A. Chakir, and J. Brion, 1995: Ozone UV spectroscopy. II. Absorption cross-sections and temperature dependence. *J. Atmos. Chem.*, **21**, 263–273, doi:10.1007/BF00696758.

McDermid, I. S., and Coauthors, 1990: Measurement intercomparison of the JPL and GSFC stratospheric ozone lidar systems. *Appl. Opt.*, **29**, 4671–4676, doi:10.1364/AO.29.004671.

McGee, T. J., D. N. Whiteman, J. J. Butler, J. F. Burris, and R. A. Ferrare, 1991: STROZ LITE: Stratospheric Ozone Lidar Trailer Experiment. *Opt. Eng.*, **30**, 31–39, doi:10.1117/12.55771.

Measures, R. M., 1984: *Laser Remote Sensing: Fundamentals and Applications*. Wiley, 510 pp.

Megie, G. J., G. Ancellet, and J. Pelon, 1985: Lidar measurements of ozone vertical profiles. *Appl. Opt.*, **24**, 3454–3463, doi:10.1364/AO.24.003454.

Mulcahy, J., C. O'Dowd, and S. Jennings, 2009: Aerosol optical depth in clean marine and continental northeast Atlantic air. *J. Geophys. Res.*, **114**, D20204, doi:10.1029/2009JD011992.

Papayannis, A., G. Ancellet, J. Pelon, and G. Mégie, 1990: Multiwavelength lidar for ozone measurements in the troposphere and the lower stratosphere. *Appl. Opt.*, **29**, 467–476, doi:10.1364/AO.29.000467.

Pliutau, D., and R. De Young, 2013: UV lidar receiver analysis for tropospheric sensing of ozone. NASA Tech. Memo. NASA/TM-2013-2018038, 18 pp.

Savitzky, A., and M. J. E. Golay, 1964: Smoothing and differentiation of data by simplified least squares procedures. *Anal. Chem.*, **36**, 1627–1639, doi:10.1021/ac60214a047.

Smit, H. G. J., and ASOPOS Panel, 2011: Quality assurance and quality control for ozonesonde measurements in GAW. Global Atmospheric Watch Rep. 201, 87 pp.

——, and Coauthors, 2007: Assessment of the performance of ECC-ozonesondes under quasi-flight conditions in the environmental simulation chamber: Insights from the Juelich Ozone Sonde Intercomparison Experiment (JOSIE). *J. Geophys. Res.*, **112**, D19306, doi:10.1029/2006JD007308.

Steinbrecht, W., T. J. McGee, L. W. Twigg, H. Claude, F. Schönenborn, G. K. Sumnicht, and D. Silbert, 2009: Intercomparison of stratospheric ozone and temperature profiles during the October 2005 Hohenpeißenberg Ozone Profiling Experiment (HOPE). *Atmos. Meas. Tech.*, **2**, 125–145, doi:10.5194/amt-2-125-2009.

Sullivan, J. T., T. J. McGee, G. K. Sumnicht, L. W. Twigg, and R. M. Hoff, 2014: A mobile differential absorption lidar to measure sub-hourly fluctuation of tropospheric ozone profiles in the Baltimore–Washington, D.C. region. *Atmos. Meas. Tech.*, **7**, 3529–3548, doi:10.5194/amt-7-3529-2014.

——, ——, T. Leblanc, G. K. Sumnicht, and L. W. Twigg, 2015: Optimization of the GSFC TROPOZ DIAL retrieval using synthetic lidar returns and ozonesondes—Part 1: Algorithm validation. *Atmos. Meas. Tech.* Discuss., **8**, 4273–4305, doi:10.5194/amtd-8-4273-2015.